JOINT INSTITUTE FOR NUCLEAR RESEARCH
Veksler and Baldin Laboratory of High Energy Physics

# FINAL REPORT ON THE START PROGRAME

Pion femtoscopy in the Zr + Zr collisions at $\sqrt{s_{\mathrm{NN}}} = 200$ GeV in the STAR experiment

**Supervisors:**

Korobitsin Artem
Nigmatkulov Grigory

**Student:**

Burov Nikolay, Moscow,
NRNU MEPhI

**Participation period:**

10 July – 02 September, 2023

Dubna, 2023

Abstract

One of the main objectives of the STAR experiment at the Relativistic Heavy Ion Collider (RHIC) is to study quark-gluon matter (QGM) produced in nuclear collisions. Spatio-temporal parameters characterizing the properties of QGM can be estimated using the method of correlation femtoscopy.

In this paper, we present an estimate of the size of the emission region of identical pions in $\mathrm{Zr}+\mathrm{Zr}$ collisions at $\sqrt{s_{NN}} = 200$ GeV. Restored the reaction plane angles and to obtain a uniform distribution the following corrections are applied: recentering and flattening. The reaction plane resolution is obtained. Dependence on the azimuthal emission angle $\Delta\Phi$ for different centralities and for transverse momentum of the pair $k_T$ is received.

CONTENTS

## Introduction

In 1956, two-particle intensity interferometry (HBT) was proposed and developed by astronomers Hanbury-Brown and Twiss to measure the angular sizes of distant stars [1]. In 1960, Goldhaber G. et al. applied this technique to elementary particle physics to study the angular distribution of identical pairs of pions in annihilations [2]. In the work, an increase in the number of pairs of identical pions born at small relative pulses was observed, which was explained by quantum statistical correlations leading to the symmetrization of the two-particle wave function. In the 1970s, Kopylov, Podhoretsky and others showed that this effect can be used to study the space-time characteristics of a system formed in collisions of particles and/or nuclei at accelerators [3, 4]. In the future, the method was called correlation femtoscopy.

In collisions of ultrarelativistic heavy ions, the formation of quark-gluon matter (QGM) is expected. To get an idea of the properties of QGM, it is necessary to know the space-time parameters that characterize it, but the small size and short duration of the reaction do not allow them to be measured directly. However, quantum-statistical correlations in the birth of particles provide a direct relationship with the size and lifetime of the source.

## Chapter 1. Theory basics

### 1.1 Correlation function of two identical particles

The two-particle correlation function is defined as the ratio of the Lorentz invariant normalized two-particle spectrum to the product of similar one-particle [5]:

$$C(\overrightarrow{p_1}, \overrightarrow{p_2}) = \frac{E_1 E_2 \frac{d^6 N_{1,2}}{d^3 p_1 d^3 p_2}}{E_1 \frac{d^3 N_1}{d^3 p_1} \cdot E_2 \frac{d^3 N_2}{d^3 p_2}}, \tag{1.1.1}$$

where $E_1$ and $E_2$ are the energy of the first and second type of particles; $N_1$ and $N_2$ are the number of born particles of the first and second type with pulses $\vec{p}_1$ and $\vec{p}_2$; $N_{1,2}$ are the number of pairs composed of particles of the first and second type with pulses $\vec{p}_1$ and $\vec{p}_2$.

Using the Wigner function $S(x, p)$, which is a function of the probability density of the birth of a particle with 4-momentum $p = (\frac{E}{c}, \vec{p})$ at the point $x = (tc, \vec{r})$, the spectra can be written as follows [5]:

$$\begin{cases} E \frac{d^3 N}{d^3 p} = \int d^4 x \, S(x, p), \\ E_1 E_2 \frac{d^6 N_{1,2}}{d^3 p_1 d^3 p_2} = \int d^4 x_1 d^4 x_2 S(x_1, x_2, p_1, p_2) |\phi(x_1, x_2, p_1, p_2)|^2 . \end{cases} \tag{1.1.2}$$

where $\phi(x_1, x_2, p_1, p_2)$ is the wave function of two born particles.

At the same time, the following assumptions are used in the calculations [6]:

1) When constructing the correlation function, only the effects of quantum statistics and the interaction in the final state are taken into account;

2) The particles descend incoherently or still imperceptibly, i.e. $S(x_1, x_2, p_1, p_2) = S_1(x_1, p_1) \cdot S_2(x_2, p_2)$;

3) Smoothness and weak impulse dependence of the Wigner function, i.e.:

$$S(x, p + \delta p) \approx S(x, p), \tag{1.1.3}$$

where $\delta p$ is a small approximation of the pulse, functional for correlates, advanced capabilities of quantum statistics and real–time interaction;

4) The identity of Wigner functions for identical particles, i.e. $S_1(x, p) \equiv S_2(x, p) \equiv S(x, p)$.

If we neglect the influence of the strong and Coulomb interaction, and leave only the contribution of the symmetrization of the free wave function of bosons, then for two pions we will have:

$$\phi(x_1, x_2, p_1, p_2) = \frac{1}{\sqrt{2}}\big(\phi(x_1, p_1)\phi(x_2, p_2) + \phi(x_1, p_2)\phi(x_2, p_1)\big). \tag{1.1.4}$$

Next, we will consider the values in the system of the center of inertia of the source, then, assuming that the pions propagate in the form of a plane wave and are emitted simultaneously, we can write:

$$|\phi(x_1, x_2, p_1, p_2)|^2 = \left|\frac{1}{\sqrt{2}}\left(e^{-ip_1x_1}e^{-ip_2x_2} + e^{-ip_2x_1}e^{-ip_1x_2}\right)\right|^2 = 1 + \cos(qr), \tag{1.1.5}$$

where the following designations are introduced $r = x_1 - x_2$ and $q = p_1 - p_2$.

By making the following variable substitution:

$$\begin{cases} k = \frac{p_1+p_2}{2}, \\ q = p_1 - p_2. \end{cases} \Longrightarrow \begin{cases} p_1 = k + \frac{q}{2}, \\ p_2 = k - \frac{q}{2}. \end{cases} \tag{1.1.6}$$

where k – pair 4-pulse

By rewriting the cosine in exponential form $\cos(qr) = \frac{e^{iqr}+e^{-iqr}}{2}$ and taking into account the above assumptions, we can obtain the correlation function of two identical pions in the following form:

$$C(\vec{q},\vec{k}) = \frac{\int d^4x_1 d^4x_2 S(x_1,x_2,p_1,p_2)|\phi(x_1,x_2,p_1,p_2)|^2}{\int d^4x_1 S_1(x_1,p_1)\int d^4x_2 S_2(x_2,p_2)} \approx \frac{\int d^4x_1 d^4x_2 S_1(x_1,p_1)S_2(x_2,p_2)|\phi(x_1,x_2,p_1,p_2)|^2}{\int d^4x_1 S_1(x_1,p_1)\int d^4x_2 S_2(x_2,p_2)} \approx$$

$$\approx 1 + \frac{\int d^4x_1 d^4x_2 S\left(x_1,k+\frac{q}{2}\right)S\left(x_2,k-\frac{q}{2}\right)\cos(qr)}{\int d^4x_1 S_1\left(x_1,k+\frac{q}{2}\right)\int d^4x_2 S_2\left(x_2,k-\frac{q}{2}\right)} = 1 + \left|\frac{\int d^4x S(x,k)e^{iqx}}{\int d^4x S(x,k)}\right|^2 = 1 + |\tilde{s}(q,k)|^2, \quad (1.1.7)$$

where $\tilde{s}(q,k) = \frac{\int d^4x S(x,k)e^{iqx}}{\int d^4x S(x,k)}$ – the normalized Fourier transform of the source function.

### 1.2 Gaussian parametrization and coordinate system

If we assume that the source has Gaussian parametrization, then the correlation function (1.1.7) will have the form [7, 8]:

$$C(\vec{q},\vec{k}) = 1 + \exp\left(-R^{\alpha\beta}(\vec{k})q_\alpha q_\beta\right), \quad \alpha,\beta = 0,1,2,3 \qquad (1.2.1)$$

where $R^{\alpha\beta}(\vec{k}) = \langle(x_\alpha - \tilde{x}_\alpha)(x_\beta - \tilde{x}_\beta)\rangle$ and the designation is entered:

$$\langle f(x)\rangle = \frac{\int d^4x S(x,k)f(x)}{\int d^4x S(x,k)} \qquad (1.2.2)$$

The simplest form of the correlation function for a Gaussian source is one-dimensional parametrization [7]:

$$C(q_{inv},\vec{k}) = 1 + e^{-q_{inv}^2 R_{inv}^2}, \qquad (1.2.3)$$

where $q_{inv}^2 = -(p_1 - p_2)^2 = -(E_1 - E_2)^2 + (\vec{p}_1 - \vec{p}_2)^2$ – the square of the relative 4 particle pulses, R_inv is the invariant radius of the emission region.

However, for a more detailed study of the spatio-temporal parameters of the QGM, a longitudinally Co-Moving coordinate system (LCMS) or the Bertsch-Pratt system is used, in which $\vec{k}_{\parallel} = 0\ \mathrm{GeV/c}$, and the first axis is longitudinal, directed along the beam axis, the second is outward, along the transverse component of the momentum of the pair $\vec{k}_T$, and the third is sideward, orthogonal to the previous two and at the same time so that the left triple is formed.

Visualization of the Bertsch-Pratt coordinate system is shown in Figure 1.1:

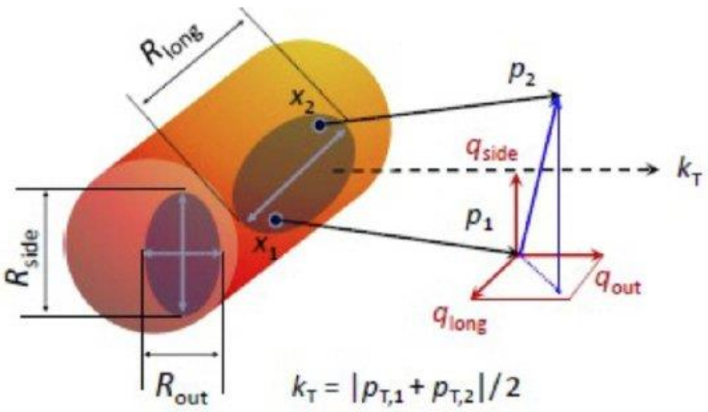


Fig. 1.1 Bertsch-Pratt coordinate system

It is assumed that for identical particles lie on the mass surface, i.e. the equalities are fulfilled:

$$\begin{cases} kq = \frac{p_1+p_2}{2}(p_1 - p_2) = \frac{p_1^2-p_2^2}{w} = \frac{m_1^2-m_2^2}{2} = 0 \\ kq = k_0 q_0 - \vec{k}\vec{q} \end{cases} \Longrightarrow q_0 = \frac{\vec{k}\vec{q}}{k_0}, \qquad (1.2.4)$$

Then the correlation function in the Bertsch-Pratt coordinate system will have the following form [8]:

$$C(\vec{q}, \vec{k}) = 1 + \exp\left(-\sum\nolimits_{i,j=o,s,l} R_{ij}^2(\vec{k}) q_i q_j\right), \qquad (1.2.5)$$

where o,s,l – abbreviations from out, side, long.

$R^2_{ij}(\vec{k})$ are given by the following expression:

$$R^2_{ij} = \langle(\hat{x}_i - \beta_i \hat{t})(\hat{x}_j - \beta_j \hat{t})\rangle, \quad i, j = out, side, long \qquad (1.2.6)$$

where $\beta_i = \frac{k_i}{k_0}$ – the speed of the pair, and the notation is introduced $\hat{x}_i = (x - \tilde{x})_i$ and $\hat{t} = (t - \tilde{t})$.

Taking into account that $\beta_{side} = \frac{k_{side}c}{E} = 0$ and $\beta_{long} = \frac{k_{long}c}{E} = 0$, the radii $R_{out}, R_{side}, R_{long}$ are given by the following formulas:

$$\begin{cases} R^2_{long} = \langle \hat{x}^2_{long} \rangle, \\ R^2_{out} = \langle (\hat{x}_{out} - \beta_\perp \hat{t})^2 \rangle,, \\ R^2_{side} = \langle \hat{x}^2_{side} \rangle, \end{cases} \qquad (1.2.7)$$

where $\beta_\perp$ – transverse component of the paired velocity.

### 1.3 Corrections for interaction in the final state

The equations for the correlation function (1.1.7), (1.2.1) and (1.2.5) were derived from the assumption that there are no interactions in the final state, namely Coulomb and strong. It is also worth considering that short-lived resonances, also generated during collisions, decay weakly at a distance of several tenths of an fm, generating pions, as a result of which correlations are muted in the experiment.

In the experiment, the following correlation function is used to adjust the experimental data taking into account the corrections for the interaction in the final state [7, 9, 10, 11]:

$$C(\vec{q}, \vec{k}) = N\left((1 - \lambda) + \lambda K_{Coul}(\vec{q})\left(1 + G(\vec{q}, \vec{k})\right)\right), \qquad (1.3.1)$$

where $N$ – normalization, $\lambda$ – a coefficient that takes into account the strength of correlations, $G(\vec{q}, \vec{k}) = \exp\left(-\sum_{i,j=o,s,l} R^2_{ij}(\vec{k}) q_i q_j\right)$ – Gaussian source function,

$K_{Coul}(\vec{q})$ – Coulomb correction, numerically calculated by the formula:

$$K_{Coul}(\vec{q},\vec{k}) = \frac{\int d^4x_1 d^4x_2 S(x_1,k) S(x_2,k) |\Psi(\vec{q},\vec{r})|^2}{\int d^4x_1 S_1(x_1,k) \int d^4x_2 S_2(x_2,k)}, \qquad (1.3.2)$$

At the same time, Sinyukov Yu.M. it was shown that the correction for the Coulomb interaction weakly depends on the size of the source [10].

The influence of the strong interaction can be taken into account in a similar way [12], however, for light particles, such as pions, and large sizes of the emitting region, it is neglected.

### 1.4 Obtaining a correlation function in an experiment

The correlation function in the experiment is obtained as follows [8]:

$$C(\vec{q},\vec{k}) = \frac{A(\vec{q})}{B(\vec{q})}, \qquad (1.4.1)$$

where $A(\vec{q})$ is the relative momentum distribution for pairs of identical pions from a single event; $B(\vec{q})$ is a similar background distribution that does not include the correlation effects of the birth of pions. This may be a distribution of non-identical pairs of pions, or a distribution of identical pairs of pions, but from different events that have the same characteristic values, such as the centrality of the collision and the position of the vertex.

## Chapter 2. STAR experiment

In the STAR experiment (Solenoidal Tracker At RHIC), which is located at the relativistic heavy ion collider (RHIC) at Brookhaven National Laboratory (BNL, USA), collisions of ultrarelativistic heavy nuclei are performed in order to obtain QGM and further study its properties and structure.

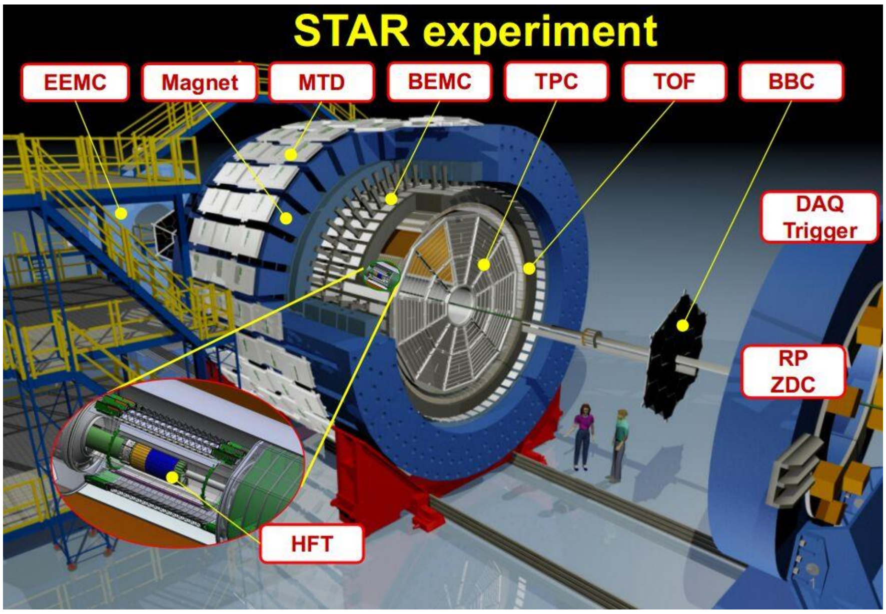


Fig. 2.1 The scheme of STAR

The experiment consists of a set of detectors [12], whose main task is to register particles formed in nuclear collisions. The data obtained using the Time Projection Chamber (TPC) and the Time of Flight system (TOF) were used in the work.

### 2.1 Time Projection Chamber

The Time-projection Chamber (TPC) is a track detector. It is one of the main detectors used in the STAR experiment, necessary for measuring the coordinates of the tracks of charged particles, as well as specific ionization losses [13]. The TPC is placed in the external field of a solenoid magnet, with a strength equal to 0.5 T [14], which makes it possible to measure the momentum of particles by the curvature of tracks in the range from $100\,\frac{\text{MeV}}{c}$ to $30\,\frac{\text{GeV}}{c}$, where $c \approx 2.997 \cdot 10^8\,\frac{m}{s}$ is the speed of light in vacuum.

Figure 2.2 schematically shows the time-projection chamber [13]:

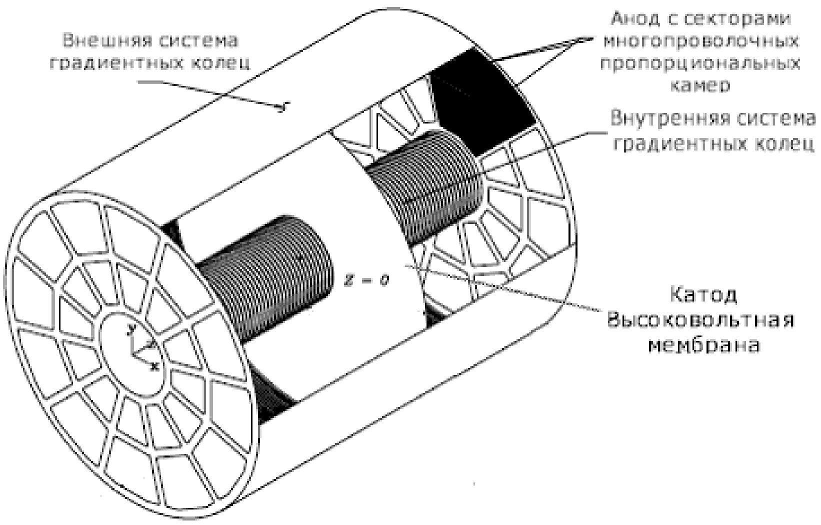


Fig. 2.2 The scheme of TPC

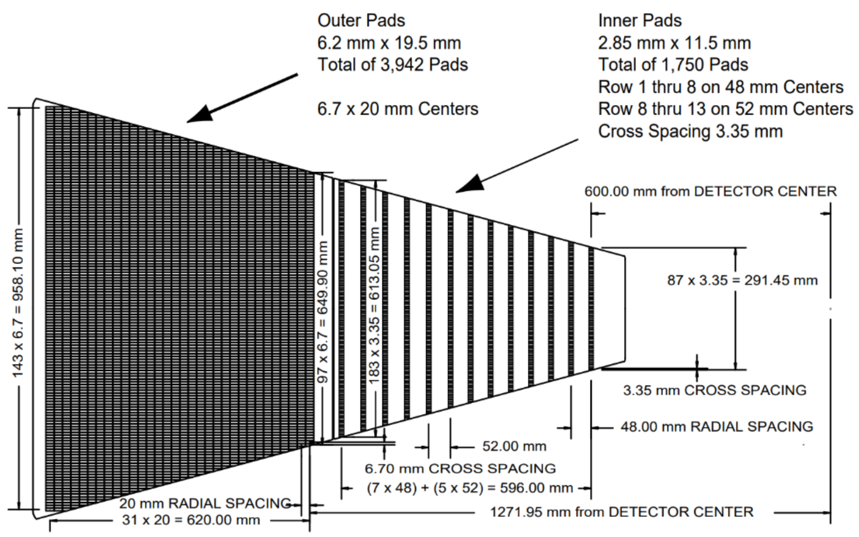


Fig. 2.3 The scheme of TPC sector

The reading ends of the TPC are divided into 12 recording sectors (Figure 2.3), each of which consists of 2 recording modules – internal and external. The internal module is necessary for a more accurate restoration of the coordinates of the beginning of the track, the external one - for collecting more electron clusters and, as a consequence, restoring the specific ionization and total energy losses of the charged particle.

Due to the fact that the specific ionization losses for π mesons, K mesons and protons for pulses greater than 700 MeV have similar values, it is not possible to identify them using only the TPC detector. Therefore, a Time-of-Flight system (TOF) is used to identify particles with large pulses.

## 2.2 Time of Flight

The TOF system consists of two separate detector systems. The first is the vertex Position Detector (VPD), which registers the collision time and the vertex coordinate along the beam axis relative to the center of the TPC. The second is the Time-of-Flight subsystem (TOFp), which registers the arrival time of the particle in the detector [15].

Figure 2.4 schematically shows the time-of-flight system [15]:

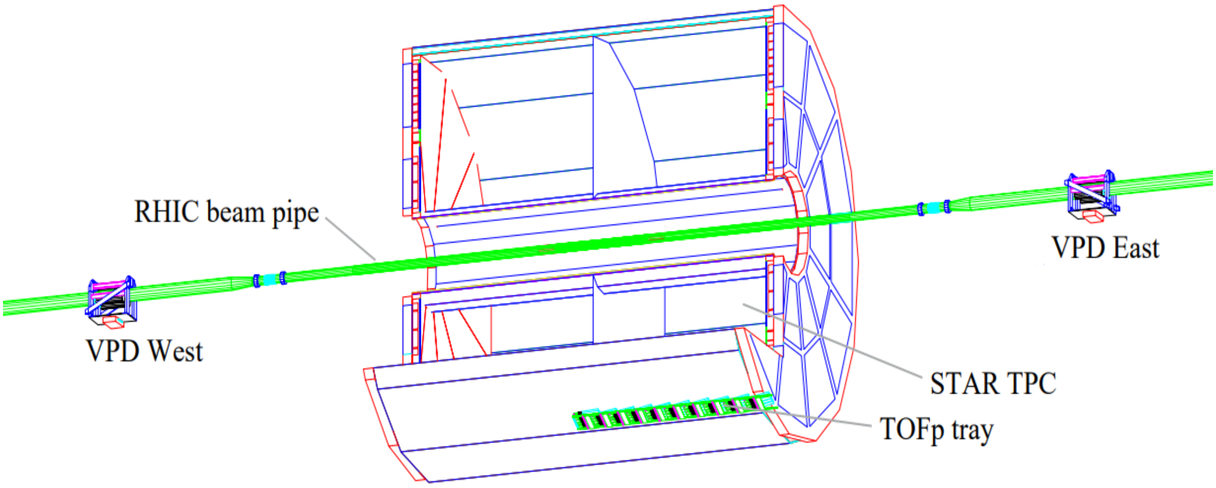


Fig. 2.4 The scheme of Time-of-Flight system

The collision time $t_{start}$ and the coordinate along the beam axis relative to the TPC $z_{vertex}$ vertex center can be determined by the following formulas [16]:

$$\begin{cases} z_{vertex} = \frac{c(t_{East} - t_{West})}{2}, \\ t_{start} = \frac{t_{East} + t_{West}}{2} - \frac{L}{c}. \end{cases} \quad (2.1)$$

where c – the speed of light, L – the distance between the "West" ("East") detector and the center TPC, $t_{West}(t_{East})$ – the time of registration of $\gamma$-quanta "West" ("East") by the detector.

To identify a particle, information about the time of flight is used, i.e. the time between its entry into a certain segment of the detector and the collision of an ion beam. Using the track information from the TPC, it is possible to determine the momentum of a particle and the length of its trajectory.

For each track registered in TOFp, you can determine the speed value β:

$$\beta = \frac{L_{track}}{c(t_{TOFp} - t_{start})}, \quad (2.2)$$

where $L_{track}$ – particle track length, $t_{start}$ – collision time, $t_{TOFp}$ – particle registration time measured by TOFp, $c$ – the speed of light.

## Chapter 3. Data analysis

The data of collisions nuclei of zirconium 96 ($^{96}_{40}Zr$) at the energy in the center of mass system per pair of nucleons $\sqrt{s_{NN}} = 200$ GeV were used in the work obtained on the STAR experiment in 2018. Events processed $\sim 30 \cdot 10^6$.

### 3.1 Selection of events, tracks and particle pairs

To select events, 2 detectors are used – TPC, to restore the position of the collision vertex (primary vertex) in space, and VPD, to separately restore the z coordinate, whose axis is directed along the beam and is counted from the center of the TPC.

Due to the fact that in the experiment the time offset between "West" and "East" VPD was not zero, so in the future we will consider those events whose z coordinate of the primary vertex belongs to the next interval: $-35.0$ cm $\leq V_z \leq 25.0$ cm.

In order to exclude incorrect reconstruction of the primary vertex, such events were selected in which the difference between the restored z coordinates of the TPC and VPD detectors modulo was no more than 5 cm: $|V_{z,TPC} - V_{z,VPD}| \leq 5$ cm and the values of each of the coordinates were greater than $10^{-5}$ cm, because if the vertex was not restored, then it was assigned values equal to 0 cm.

At the same time, in order to reduce the influence of the background from events related to the interaction of the beam and the walls of the collider tube, a restriction on the radial component of the primary vertex is introduced: $|V_r| \leq 2$ cm.

Final cuts for events:

$$\begin{cases} V_x, V_y, V_z \geq 10^{-5}\text{cm}, \\ -35.0\ \text{см} \leq V_{z,TPC} \leq 25.0\ \text{cm}, \\ \left|V_{z,TPC} - V_{z,VPD}\right| \leq 5\ \text{cm}, \\ |V_r| = \sqrt{V_x^2 + V_y^2} \leq 2\ \text{cm}. \end{cases} \quad (3.1.1)$$

Due to the finite resolution and geometric features of the TPC detector and the imperfection of reconstruction methods, for the most accurate recovery and reduction of data contamination by secondary charged particles, it is necessary that the track parameters satisfy the following restrictions:

$$\begin{cases} \text{nHits} \geq 16, \\ \dfrac{\text{nHits}}{\text{nHitsPoss}} \geq\ 0.51, \\ |\eta| \leq 1, \end{cases} \quad (3.1.2)$$

where nHits – the number of registered electronic clusters used in the reconstruction of tracks (hits); nHitsPoss – the number of registered electronic clusters that may belong to this track; $\eta$ – pseudorapidity.

The identification of particles takes place on the basis of specific ionization losses measured using the TPC detector and arising from the passage of a charged particle through a substance.

At the same time, in order to find the size of the emission region using correlation femtoscopy, it is necessary that the particles originate from the region of space in which the collision of heavy ions occurred, for this the tracks must be primary.

The selection of pions with higher values of the pulse modulus only by the TPC detector is complicated by the fact that for some types of particles the graphs of specific ionization losses have intersections, therefore, for more accurate identification it is also necessary to use the TOF detector.

The final criteria for the selection of peonies using two types of identification – TPC and TOF, are presented in the table 3.1.

Table 3.1 Final cuts for tracks

<table>
<tr><td colspan="2">$\mathrm{nHits} \geq 16$</td></tr>
<tr><td colspan="2">$\frac{\mathrm{nHits}}{\mathrm{nHitsPoss}} \geq 0.51$</td></tr>
<tr><td colspan="2">$\lvert\eta\rvert \leq 1$</td></tr>
<tr><td colspan="2">Primary tracks</td></tr>
<tr><td>TPC:</td><td>TPC & TOF:</td></tr>
<tr><td>$\lvert n\sigma_{\pi}\rvert \leq 2$</td><td>$\lvert n\sigma_{\pi}\rvert \leq 3$</td></tr>
<tr><td rowspan="2">$0.15\ \mathrm{GeV/c} \leq \lvert\vec{\mathrm{p}}\rvert \leq 0.60\ \mathrm{GeV/c}$</td><td>$-0.015 \leq \left(\frac{1}{\beta_{\mathrm{i}}} - \frac{1}{\beta_{\pi}}\right) \leq 0.015$</td></tr>
<tr><td>$0.60\ \mathrm{GeV/c} \leq \lvert\vec{\mathrm{p}}\rvert \leq 1.80\ \mathrm{GeV/c}$</td></tr>
</table>

In correlation femtoscopy, pairs of particles born with close pulses are the main objects of research, therefore, the effects associated with incorrect reconstruction of tracks, namely, the splitting of one track into two and the merging of two tracks into one, are the main sources of measurement inaccuracy.

To reduce the effect of splitting and merging, restrictions are introduced on the values called Splitting Level (SL) and Fraction of Merging Row (FMR).

Final cuts for particle pairs:

$$\begin{cases} -0.5 \leq SL \leq 0.6, \\ -1.0 \leq FMR \leq 0.1, \end{cases} \tag{3.1.3}$$

### 3.2 Reconstruction of reaction plane angle

In this work, the reaction plane angles recovered using the TPC detector were used. Therefore, in order to avoid correlations of the particle birth angle and the angle of the reaction plane, the TPC detector was divided into 2 parts: West ($\eta \geq 0$) and East ($\eta < 0$). At the same time, during the analysis, the spectra of particle pairs from West (East) TPC were plotted relative to the angle from East (West) TPC.

To reconstruct the reaction plane angle a Q-vector is used, the components of which are given by the expression [17, 18]:

$$\begin{cases} Q_x = \sum_i p_t \cos(2\phi), \\ Q_y = \sum_i p_t \sin(2\phi), \end{cases} \tag{3.2.1}$$

where $p_t$ – transverse momentum of the particle; $\phi$ – the azimuth angle of the particle in the TPC coordinate system.

Then the angle of the reaction plane can be found using the following expression [f:

$$\Psi_2 = \frac{1}{2}\arctan\left(\frac{Q_y}{Q_x}\right), \tag{3.2.2}$$

At the same time, due to the symmetry of the experiment, the distribution of the angle of the reaction plane over the events should be uniform. However, in the experiment, due to the imperfection of the detectors, this is not the case. Therefore, the following corrections are applied to obtain a uniform distribution [19, 20]:

1. Recentering - one subtracts from the Q-vector of each event, the Q-vector averaged over many events: $Q^1 = Q^0 - \langle Q^0 \rangle$, where $Q^0$ and $Q^1$ – Q-vector before and after correction. Averaging is carried out for all events.

2. Flattening – fit the non-flat distributions of the reaction plane angle to a Fourier expansion and to apply an event-by-event shifting of the reaction planes in order to make the final distributions isotropic [20, 21]:

$$\begin{cases} \Psi_2^2 = \Psi_2^1 + \Delta\Psi_2^1, \\ \Delta\Psi_2^1 = \frac{1}{2}\sum_{m=1}^{m_{max}} \frac{2}{m}\left(\langle \sin(2m\Psi_2^1)\rangle \cos(2m\Psi_2^1) + \langle \cos(2m\Psi_2^1)\rangle \sin(2m\Psi_2^1)\right), \end{cases} \quad (3.2.3)$$

where $\Psi_2^1$ and $\Psi_2^2$ – reaction plane angle before and after correction;

An example of the distribution of the reaction plane angle before and after correction for a centrality $10 - 30$ % and East TPC is shown in the Figure 3.1 :

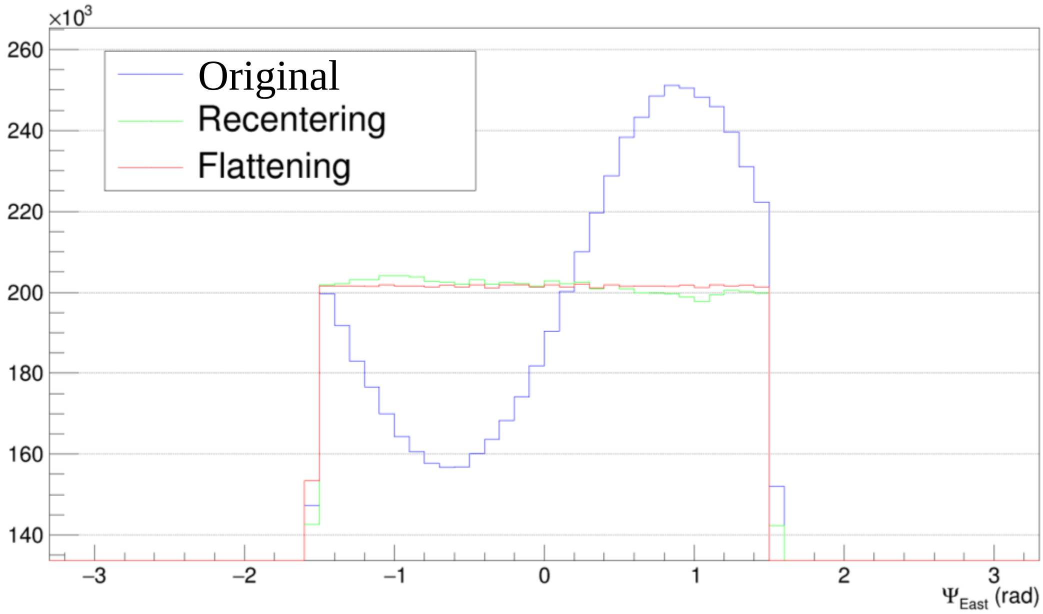


Fig. 3.1 Distribution of the reaction plane angle

The Fourier expansion used the first 10 terms. As you can see, after all the corrections, the distribution became uniform.

### 3.3 The reaction plane resolution

Because the position of the true reaction plane is not known a priori, one can only perform Fourier decomposition of the invariant particle distribution $E\frac{d^3N}{d^3p}$ with respect to the reconstructed position of the reaction plane $\Psi_n$ where n is the order of the harmonic from which this position is reconstructed. Due to the finite multiplicity, the difference between the true and the reconstructed reaction plane is not zero. Thus, the obtained distributions must be adjusted taking into account the resolution of the reaction plane. The resolution of the reaction plane is given by the formula [20]:

$$\mathrm{Res} = \sqrt{2\left\langle \cos\left(\mathrm{n}\left(\Psi_{\mathrm{n,East}} - \Psi_{\mathrm{n,West}}\right)\right)\right\rangle}, \quad (3.3.1)$$

The obtained dependence of the reaction plane resolution on the centrality is shown in the figure 3.2:

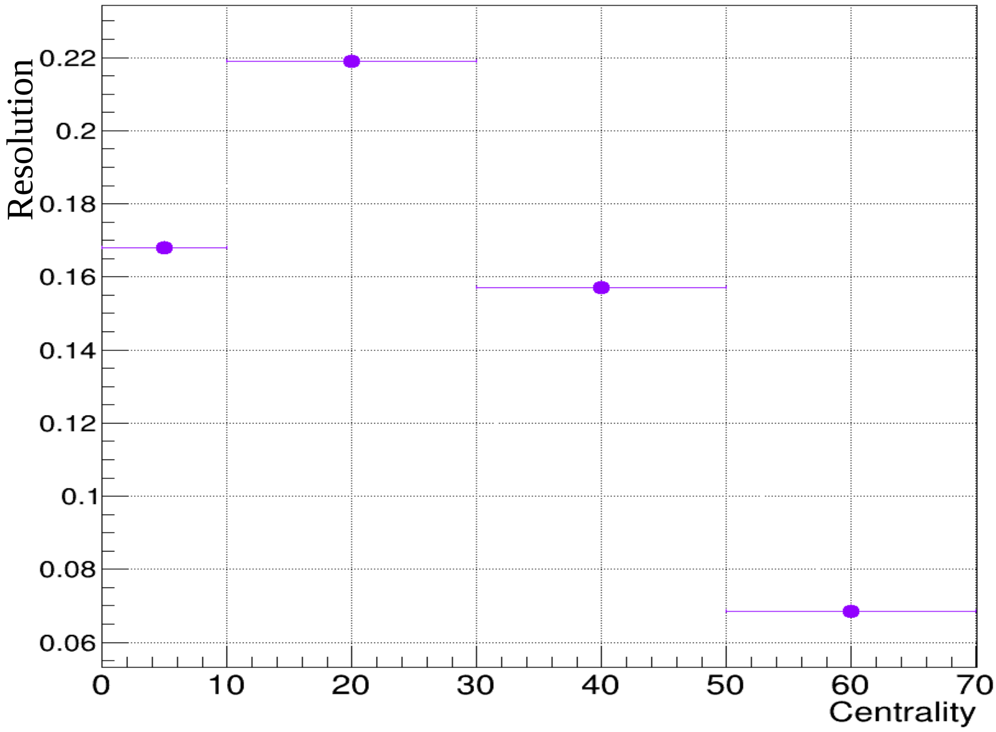


Fig. 3.2 Reaction plane resolution

As you can see, the reaction plane resolution has a maximum at a centrality of $10 - 30$ %.

## Chapter 4. Dependences of femtoscopic radii on the relative angle of emission of a particle pair

Having extracted the orientation of the reaction plane from the final distribution of the emitted particle momenta, one can then address the question of their spatial distribution relative to the reaction plane by measuring two-particle correlations as a function of the azimuthal emission angle $\Delta\Phi$ (i.e. the direction of the transverse momentum vector $\vec{k}_T$ of the emitted particle pairs relative to reaction plane angle). Complementing the spectral information on the momentum-space structure of the source with space-time information from the correlation functions severely constrains models for the dynamical evolution of the reaction zone. For noncentral collisions interesting questions that can be addressed in this way are the origin and manifestation of anisotropic collective flow and its consequences for the space-time evolution of the fireball, from which information about the intensity of rescattering effects and the degree of thermalization in particular during the early stages of the collision can be extracted

To study the dependence of the size of the particle emission region, three-dimensional correlation functions for collision centralities:$0-10$, $10-30$, $30-50$, $50-70$ %, and for the transverse momentum of the pair $k_T$: $0.10 - 0.20$, $0.20-0.30$, $0.30-0.40$, $0.40-0.50$, $0.50-0.60$ GeV/c depending on the azimuthal emission angle $\Delta\Phi$ were constructed.

To fit to the obtained distributions and, as a consequence, to extract the size of the emission region, the correlation function of the Gaussian source was used, taking into account the correction for the Coulomb interaction of particles in the final state, which is given by the equation (1.3.1).

An example of one-dimensional projections of some of the obtained correlation functions together with their fit is shown in Figure 4.1:

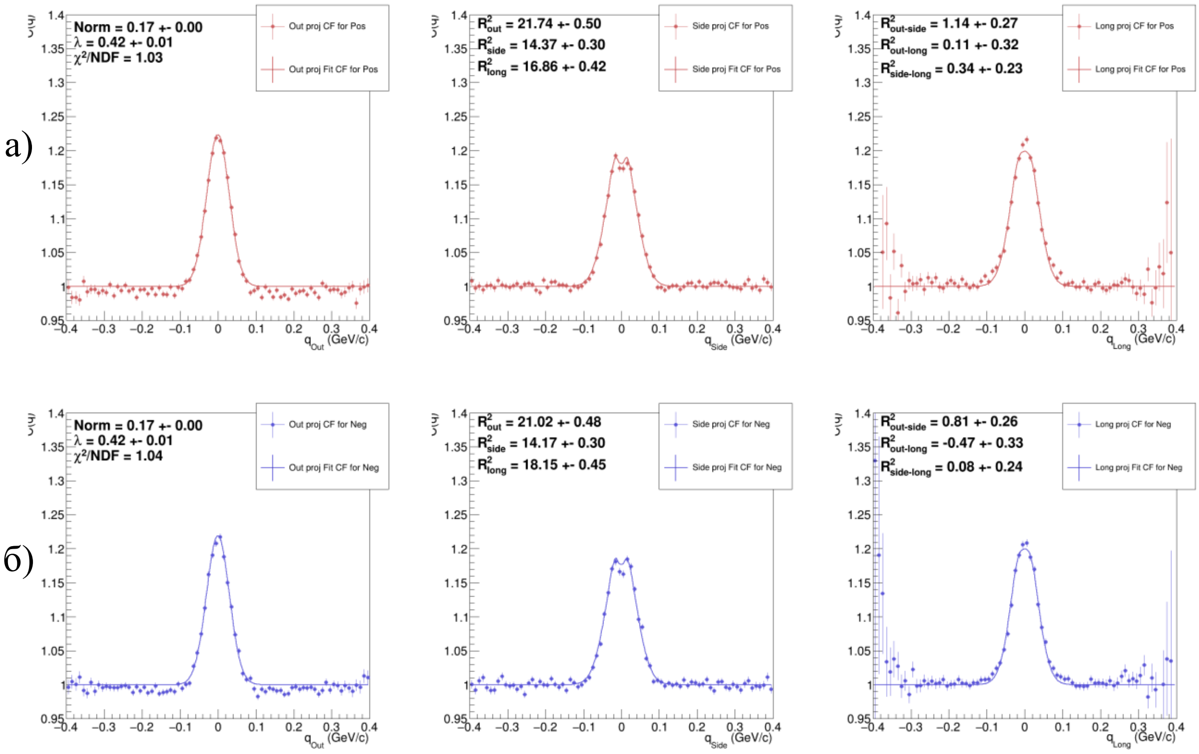


Fig. 4.1 Projections of the correlation function for the centrality of 0-10%, the momentum $k_T = 0.30 - 0.40$ GeV/c and the azimuthal emission angle $\Delta\Phi = \frac{\pi}{8} - \frac{\pi}{4}$ for a) positively and b) negatively charged pions.

At the same time, the correlation functions for positively and negatively charged pions were compared by searching for the ratio $\frac{C_{\pi^+\pi^+}(q_{out}, q_{side}, q_{long})}{C_{\pi^-\pi^-}(q_{out}, q_{side}, q_{long})}$. The resulting distributions are shown in Figure 4.2.

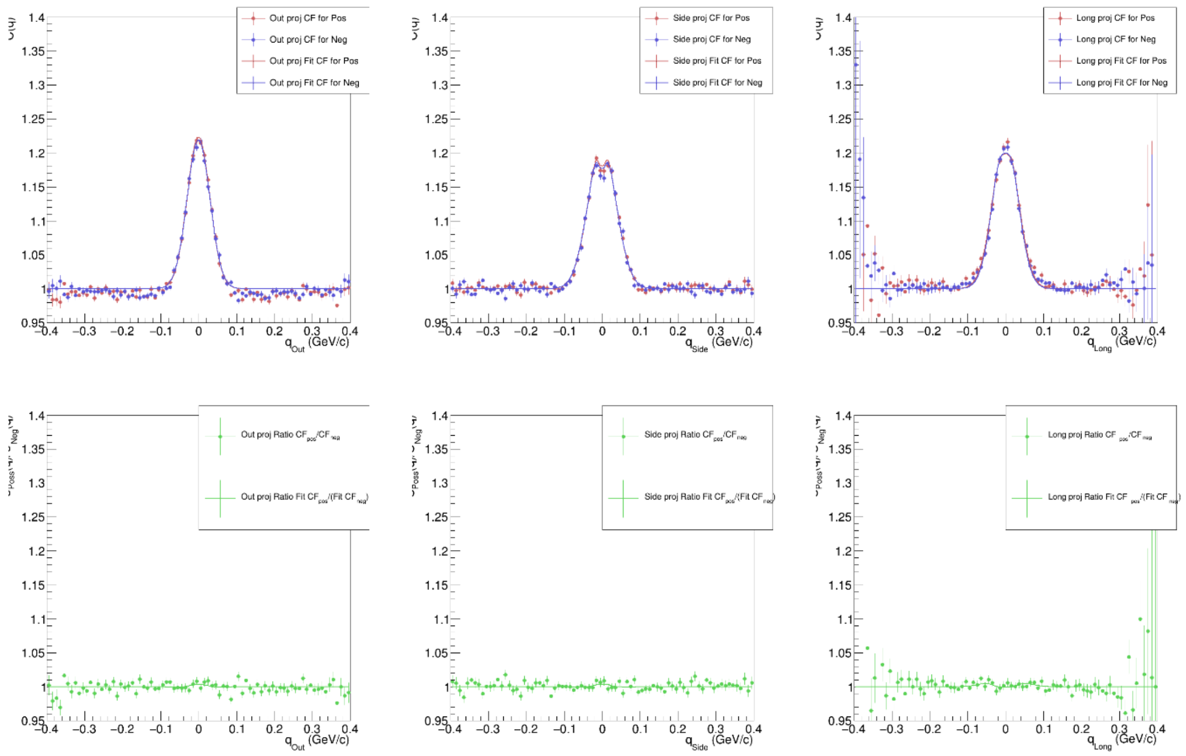


Fig. 4.2 a) Correlation functions for the centrality of 0-10%, the momentum $k_T = 0.30 - 0.40$ GeV/c and the azimuthal emission angle $\Delta\Phi = \frac{\pi}{8} - \frac{\pi}{4}$ for positive and negative pions with their fits. b) Their attitude.

As can be seen from the relations in Figure 4.2, the difference between the correlation functions for positive and negative pions is less than 1%.

The dependence of femtoscopic parameters on the azimuthal emission angle $\Delta\Phi$ for different centralities and transverse momentum of the pair $\vec{k}_T$ obtained by fitting is shown in Figures 4.3-4.4.

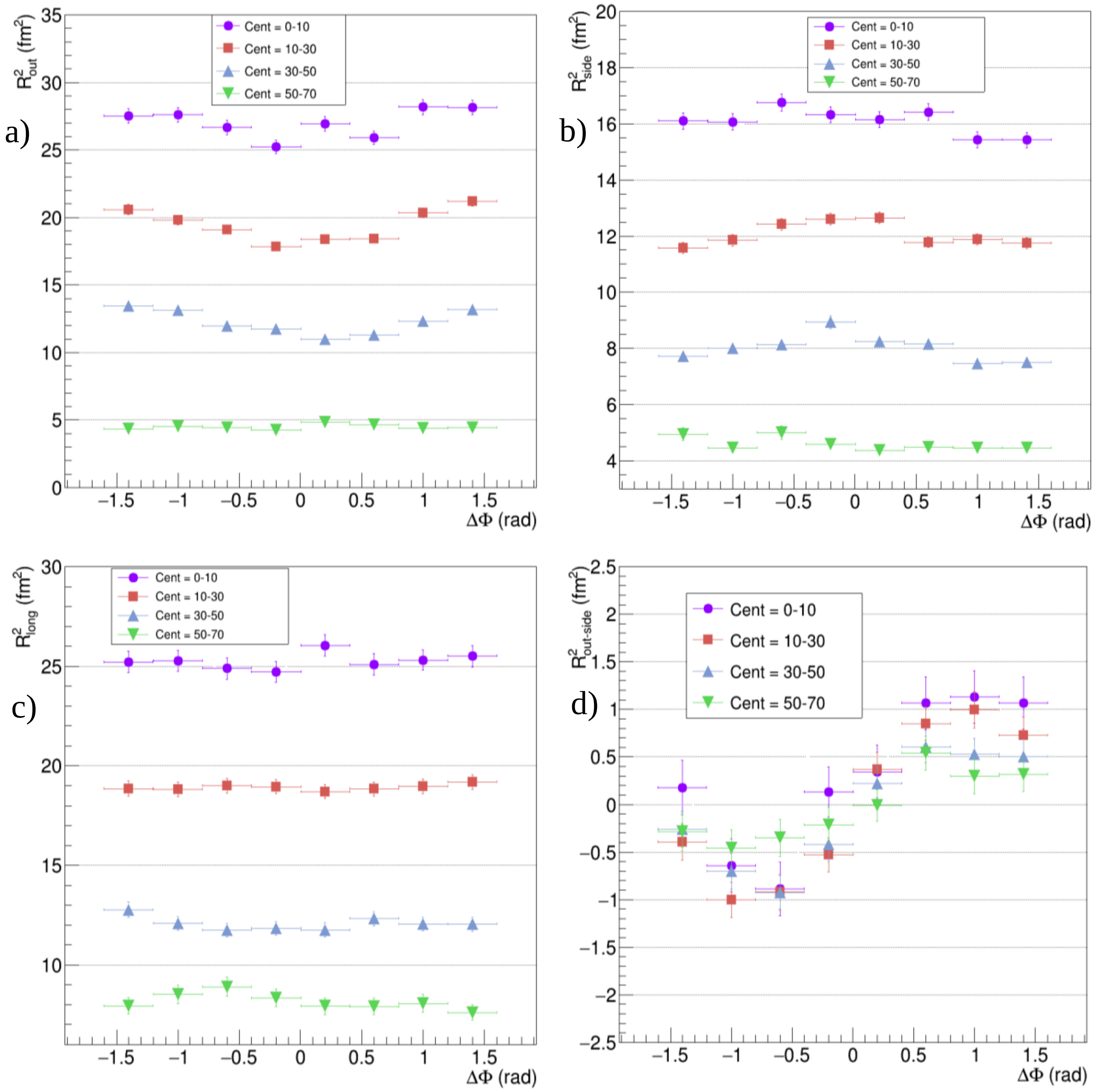


Fig. 4.3 The dependence a) $R^2_{out}$, b) $R^2_{side}$, c) $R^2_{long}$, d) $R^2_{out-side}$ on the azimuthal emission angle $\Delta\Phi$ for different centralities.

As can be seen from the dependencies, the size of the particle emission region decreases with increasing centrality. This is due to a decrease in the overlap area of colliding nuclei and, as a consequence, the number of nucleons interacting in the reaction.

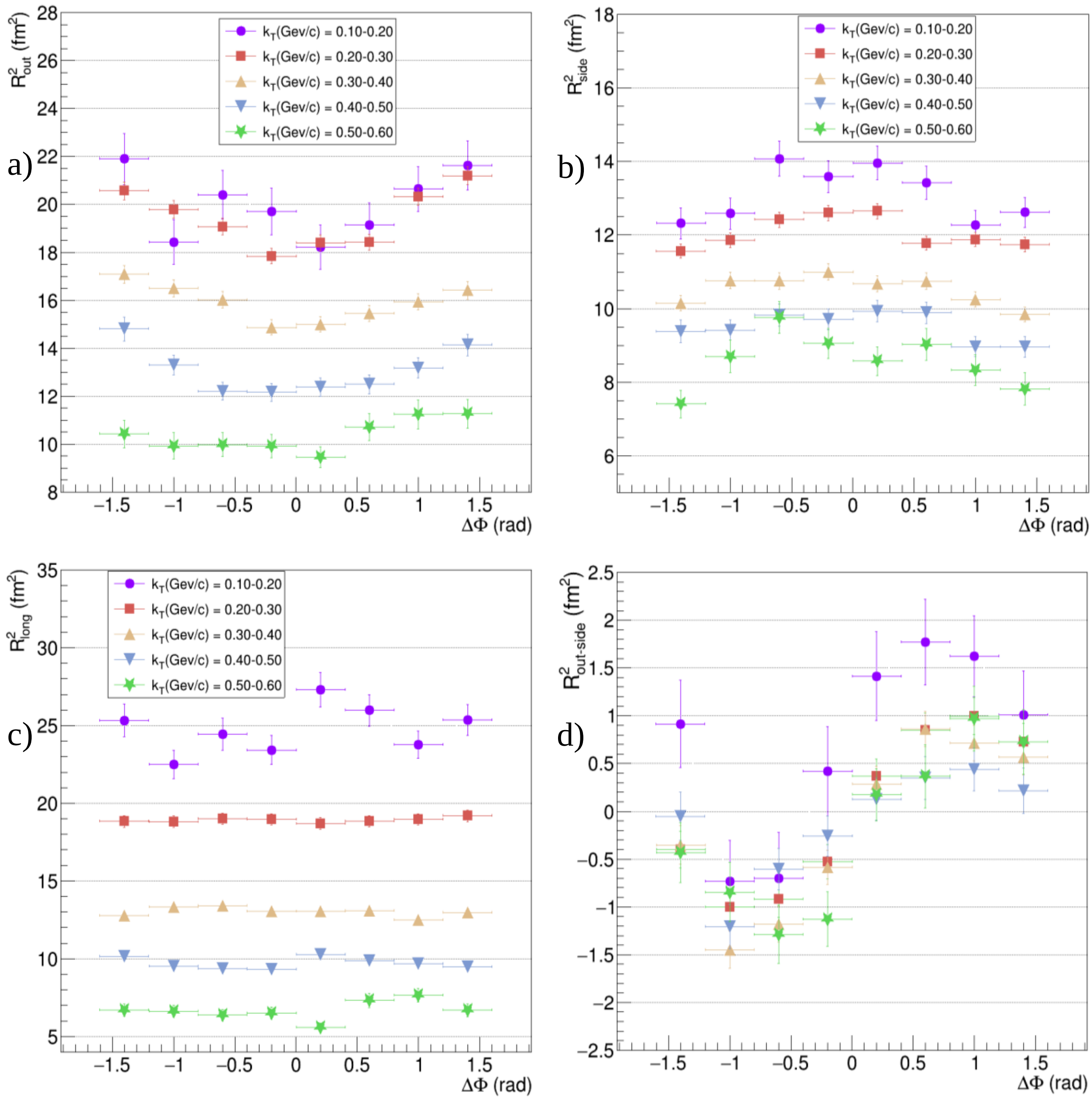


Fig. 4.3 The dependence a) $\mathrm{R}^2_{\mathrm{out}}$, b) $\mathrm{R}^2_{\mathrm{side}}$, c) $\mathrm{R}^2_{\mathrm{long}}$, d) $\mathrm{R}^2_{\mathrm{out-side}}$ on the azimuthal emission angle $\Delta\Phi$ for different pair momentum $\vec{\mathrm{k}}_{\mathrm{T}}$.

The size reduction with the help of an impulse pair can be explained by the presence of collective flows. [22, 23, 24].

## Conclusion

In this work, data on collisions of zirconium nuclei $\mathrm{Zr} + \mathrm{Zr}$ at the energy in the center of mass system per pair of nucleons $\sqrt{s_{NN}} = 200$ GeV were processed obtained in the STAR experiment in 2018.

The reaction plane angles of the second order $\Psi_2$ are restored. To obtain a uniform distribution of the reaction plane angle, correction methods were applied: recentering and flattening. Also, the reaction plane resolution is obtained.

Three-dimensional distributions of the relative momentum $\vec{q} = (q_{out}, q_{side}, q_{long})$ for collision centralities: $0 - 10$, $10 - 30$, $30 - 50$, $50 - 70$ %, and for transverse momentum of the pair $k_T$: $0.10 - 0.20$, $0.20 - 0.30$, $0.30 - 0.40$, $0.40 - 0.50$, $0.50 - 0.60$ GeV/c depending on the azimuthal emission angle $\Delta\Phi$ were obtained.

By adjusting the correlation function of the Gaussian source, taking into account the correction for the Coulomb interaction of particles in the final state to the obtained distributions, the size of the emitting region was estimated. Their dependence on the azimuthal emission angle $\Delta\Phi$ for different centralities and for transverse momentum of the pair $k_T$ is also investigated.

**Reference**

1. Hanbery Brown R., Twiss R. A Test of a New Type of Stellar Interferometer on Sirius // Nature. − 1956. − Vol. 178. − P. 1046-1048.

2. Goldhaber G., Goldhaber S., Wonyong L., Abraham P. Influence of Bose-Einstein statistics on the anti-proton proton annihilation process // Phys. Rev. — 1960. — Vol. 120. — P. 300-312.

3. Kopylov, G. I. Correlations of identical particles emitted by highly excited nuclei // Soviet Journal of Nuclear Physics. – 1972. - Vol. 15. - P. 219-223.

4. Kopylov, G. I. Like particle correlations as a tool to study the multiple production mechanism // Physical Letters B. - 1974. - Vol.50. - P. 472-474.

5. Heinz U. Two-Particle Correaltions in Relativistic Heavy-Ion Collisions // Annual Review of Nuclear and Particle Science. – 1999. – Vol. 49. – P. 529-579.

6. Lednicky R. Correlation femtoscopy // Nuclear Physics A. – 2006. – Vol. 774. – P. 189-198.

7. Tomasik B. and Wiedemann A. Central and Non-central HBT from AGS to RHIC // Quark–Gluon Plasma 3. – 2004. – Vol. 3. – P. 715-777.

8. Lisa M. Femtoscopy in Relativistic Heavy Ion Collisions: Two Decades of Progress // Annual Review of Nuclear and Particle Science. – 2005. – V. 55 – P. 357-402.

9. Sinyukov Yu.M., Lednicky. R., Pluta. J. and Erazmus B. Coulomb Corrections for Interferometry Analysis of Expanding Hadron Systems // Physics Letters B. – 1998. – Vol. 432. – P. 248-257.

10. Bowler M. Coulomb corrections to Bose-Einstein correlations have been greatly exaggerated // Physics Letters B. – 1991. – Vol. 270. – P. 69-74.

11. Koonin S.E. Proton pictures of high-energy nuclear collisions// Physics Letters B. – 1977. – Vol. 70. – P. 43-47.

12. Conceptual design report for the Solenoidal Tracker at RHIC – United States: N.p., 1992. – P. 346. – Web. doi:10.2172/10180669.

13. Anderson M. et al. The STAR time projection chamber: a unique tool for

studying high multiplicity events at RHIC // Nuclear Instruments and Methods in Physics Research A. – 2003. – Vol. 499 – P. 659-678.

14. Brown R.L. et al. The STAR Detector Magnet Subsystem // Particle Accelerator Conference. – Vancouver, 1997. – P. 5.

15. Llope W.J. et al. The TOFp and pVPD Time-of-Flight System for STAR // Nuclear Instruments and Methods in Physics Research A. – 2004. – Vol. 522. – P. 252-273.

16. Llope W.J. et al. The STAR Vertex Position Detector // Nuclear Instruments and Methods in Physics Research A. – 2014. – Vol. 759. – P. 23-28.

17. Voloshin S., Zhang Y. Flow study in Relativistic nuclear collisions by Fourier expansion of azimuthal particle distributions // Z Phys C – Particles and Fields. – 1996. – Vol. 70 – P. 665-671.

18. Poskanzer A. and Voloshin S. Methods for analyzing anisotropic flow in relativistic nuclear collisions // Physical Review C. – 1998. – Vol. 58. – P. 1671-1678.

19. Voloshin S., Poskanzer M. and Shelling R. Collective phenomena in non-central nuclear collisions // Relativistic Heavy Ion Physics. – 2008. - Vol. 23. – P. 293-347/

20. Milosevic J. Investigation of azimuthal asymmetries in charged and strange particle distributions from CERES // Cern-Thesis. – 2005. – Vol. – P. 115.

21. Barrette J. et al. Proton and pion production relative to the reaction plane in Au+Au collisions at 11A GeV/c // Physical Review C. – 1997. – Vol. 54. – P. 3254-3264.

22. Adamczyk L. Beam-energy-dependent two-pion interferometry and the freeze-out eccentricity of pions measured in heavy ion collisions at the STAR detector // Physical Review C. – 2015. – Vol. 92. – P. 014904-1–014904-27.

23. Akkelin S.V. and Sinyukov Y.M. The HBT-interferometry of expanding sources // Physics Letters B. – 1995. – Vol. 356. – P. 525-530.

24. Lisa M. Femtoscopy in heavy ion collisions. Wherefore, whence, and whither? // AIP Conference Proceedings. – 2006. – Vol. 828. – P. 226-237.